Microscale model comparison (benchmark) at the moderate complex forested site Ryningsnäs

Stefan Ivanell[1], Johan Arnqvist[1], Matias Avila[2], Dalibor Cavar[3], Roberto Aurelio Chavez-Arroyo[4], Hugo Olivares-Espinosa[1], Carlos Peralta[5], Jamal Adib[5], and Björn Witha[6]

[1]Uppsala University, Wind Energy Section, Campus Gotland, 621 67 Visby, Sweden
[2]Barcelona Supercomputing Center, BSC, Spain
[3]Wind Energy Department, Technical University of Denmark, Denmark
[4]National Renewable Energy Centre (CENER), Spain
[5]Wobben Research and Development MS GmbH, Germany
[6]ForWind - Carl von Ossietzky Universität Oldenburg, Germany

Correspondence to: Stefan Ivanell (stefan.ivanell@geo.uu.se)

Abstract. This article describes a study where modellers were challenged to compute the wind at a forested site with moderately complex topography. The target was to match the measured wind profile at one exact location for three directions. The input to the modellers consisted of detailed information of forest densities and ground height derived from Airborne Laser Scans (ALS). All participating models except two used the full detailed ground and forest information to model the forest which is considered a significant progress. The ALS based data resulted in reasonable agreement of the wind profile and turbulence magnitude. The best performance was found to be that of LES using a very large domain. For the RANS type of models the constants in the turbulence closure was shown to be of great significance for the turbulence level, but of much less importance for the wind speed profile. Overall, the article gives an overview of how well different types of models are able to capture the flow physics at a moderate complex forested site.

10 *Copyright statement.* TEXT

1 Introduction

To encounter the increasing demand of wind power, new areas are explored. Large off-shore farms further away from the shore are being developed as well as wind farms in more complex areas on-shore, such as terrain with more complex topology and roughness. In northern countries, for example Scandinavia, large remote forested areas are being explored. However, when
15 exploring these complex sites it is evident that new challenges arise due to turbulence level and wind shear Enevoldsen (2016).

In addition to the actual difference in wind climate between traditional wind energy sites and complex forested ones, modelling of the wind conditions is challenging. Trees are elevated sources for both momentum absorption and heat transfer and thus they differ from traditional surfaces since the exchange may be distributed at several model levels. The degree of physical description is a choice by the modeller, going from describing Plant Area Densities (PAD) in each grid cell to representing

an entire forest by a single roughness length value. The required numerical demand does however vary with many orders of magnitude when making that choice.

There are not to the authors knowledge any large scale studies comparing different micro scale models over forested terrain with high quality meteorological data. However, Ayotte (2008) compared models of varying complexity to wind tunnel

5 measurements and concluded that inaccurate representation of all physical scales may result in significant errors. So far there remains significant uncertainties in the skill wind climate model performance in forested areas, and there are also large differences between model descriptions. Hence there is a need for more validation studies and a better understanding of how different modelling choices affects the end result. This study aims to take the first steps to fill that knowledge gap by presenting model performances at a forested wind turbine site.

10 The study started with a call for a benchmarking model validation study to modellers involved in the European ERANET+ project New European Wind Atlas (NEWA). The aim with the benchmark is to illustrate how well micro-scale models are able to simulate winds above a forest in medium complex topography. The models used scopes from industrial wind models to the frontline research approaches. The modelled case consists of a typical site located in Ryningnäs in southern Sweden, i.e., a patchy forested site with moderate topography Arnqvist et al. (2015).

15 The NEWA project includes several large scale field campaigns designed for flow model validation Mann et al. (2017), however, the Ryningnäs measurements campaign was performed prior to the start of NEWA project and was identified as an appropriate dataset for a benchmarking study. As such it also forms a basis for model validation methodology as preparation for coming benchmarks using measurement input from the extensive measurements campaigns performed within the NEWA project.

20 The progress of forest flow modelling now enables direct simulation of the tree densities. Such density, PAD, may be derived from Airborne Laser Scans (ALS) that are becoming increasingly available from national map services Boudreault et al. (2015). Using PAD data instead of estimated roughness lengths may be a way to reduce the uncertainties of site assessment and in order to the test the performance of wind determined by models using PAD derived from ALS such data was made available to the modellers talking part in the study.

25 The study consists of a blindtest benchmark comparing model performance with measurements from three different wind directions under neutral conditions for a patchy forested site in Sweden. The paper begins with descriptive parts; the benchmark, the validation data, general modelling followed by description of first the RANS models and then the LES models. It then continues with the main results and finally concludes with a discussion and conclusions section.

2 Benchmark description

30 The benchmark task was to model the wind profile at the location $57°16'34.26"$N, $15°59'12.23"$E for the wind directions $100°$, $240°$ and $290°$ (directions referring to 100 m height). The input provided to the modellers was a target wind speed of 7.4 ms^{-1} at 100 m height, neutral atmospheric stratification and a data set of forest density and topography in a 40 km $\times$40 km

grid. The modellers were asked to provide the wind profile from the ground up to at least 200 m, geostrophic wind speed U_g, wind speed in planes at 40, 100 and 140 m above local ground level (AGL) as well as information of their model.

3 Measurements

3.1 Forest characterisation by laser scans

5 In order to characterise the forest ALS data from the Swedish map authority Lantmäteriet has been utilised Lantmäteriet (2016). The data was collected at a flight height of 1700 m yielding a foot print area at the ground of 0.5 m² for the laser beam. The density is around 1 shot/m². The data was processed according the method described in Boudreault (2015). The method uses Beer-Lambert law for the attenuation of the laser beam as it travels through the forest canopy and the Plant Area Density (PAD) can be derived if the extinction coefficient is known. The extinction coefficient was here (as in Boudreault (2015)) assumed

10 to be $0.5/cos(\theta_{ALS})$, where θ_{ALS} is the scanning angle, corresponding to a spherical distribution of canopy elements. The height of the forest was derived by the maximum return height in a grid box as defined by the distance from the median of the returns in that grid box that had been classified as ground (a.k.a. the ground height of the grid box). The PAD was derived in vertical steps of 1 m from the highest return reflection towards the ground. In order to avoid numerical problems when the beam becomes fully attenuated (in very dense forest patches) PAD estimation was terminated if less than 5% of the points

15 remained to the levels below. Two data sets of resolution 10 m by 10 m and 50 m by 50 m respectively were then prepared to be used as model input. The data sets include horizontal coordinates, ground height, tree height and PAD in a vertical grid from 0 m above ground to the tree height in steps of 1 m.

3.2 Site description

The measurement site is located in Ryningsnäs in south-east Sweden (57°16′34.26"N, 15°59′12.23"E). A 138 m high mea-

20 surement tower equipped with cup and sonic anemometers has been used for the validation data. The area around the tower site has moderate complexity in terms of topography, but the forest cover is very heterogeneous with many clearings and stands of different age. Fig 1 shows the forest cover on different scales, the largest being 50 km by 50 km and the smallest 1 km by 1 km. The three sectors chosen for the validation study have been highlighted by colouring.

The tower is situated in the north-west corner of a clearing of around 400 m ×400 m. The surrounding forest has a peak in

25 the tree height distribution at approximately 20 m and is predominantly consisting of Scotts Pine (*Pinus Sylvestris*). The actual tree height distribution can be seen in Fig. 2 (*a*) and (*b*) where the distribution is shown for the three sectors within a radius of 10 km (*a*) and 1 km (*b*). In the larger scale, the tree height distributions of sectors 100° and 240° are very similar with a peak at 21.5 m. The distribution of sector 290° is more flat, with two maximums, one at 7.5 m and one at 19.5 m. In the closer region the 290° distribution is different from the two other sectors in that it does not contain a clearing, but does contain a large

30 patch of young forest at 7.5 m height. The clearing of the tower itself can be seen in the distribution of the 100° sector whereas the clearing in the 240° sector is almost one km upwind.
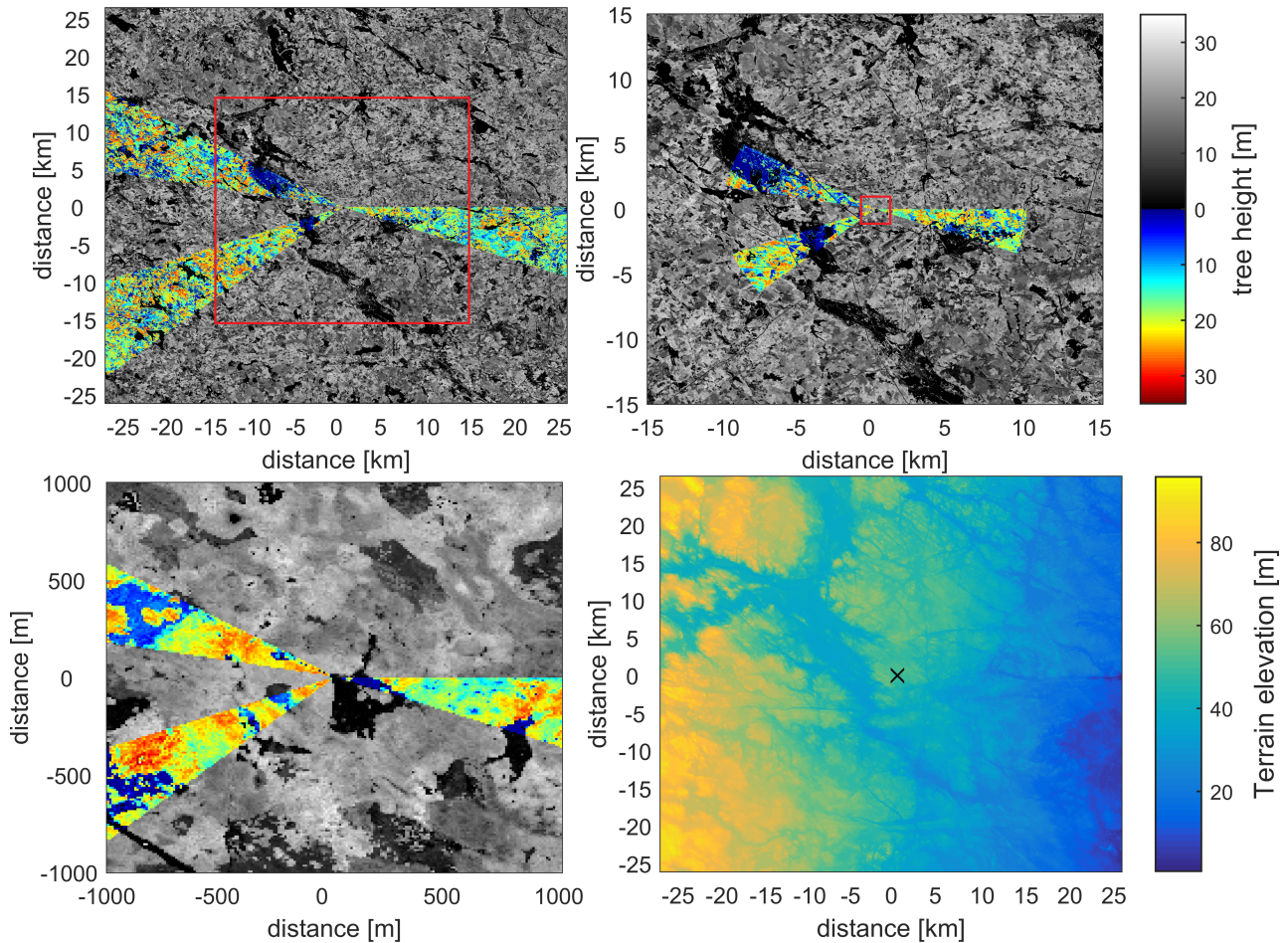
Figure 1. $(a) - (c)$ Forest cover of the Ryningsnäs site with increasing magnification factors. The contour map in grey scale and colour scale illustrate the tree height distribution, both inside and outside the selected area. (d) A topographic map of the Ryningsnäs area.

Two wind turbines are situated approximately 200 m to the north east and south of the tower respectively, but the three sectors used in the validation study exclude directions from which the turbine has influence.

3.3 Wind measurements

The full measurement set up and the wind climate has earlier been reported in Arnqvist et al. (2015). The instruments used in this study includes six sonic anemometers (Metek Gmbh, USA-1) located at the heights of 40, 59, 80, 98, 120 and 137.7 meters as well as 7 Thies first-class cup anemometers at the heights 25.5, 40.1, 60.5, 80.1, 95.85, 120.75 and 137.6 m.

The sonics where sampled at 20 Hz and statistics was evaluated by 30 minute block averaging and 3D rotation of the coordinate system aligning it with the local mean wind direction yielding the wind vector $\bar{u}$, $\bar{v}$, $\bar{w}$ and temperature $\bar{t}$. Flow distortion correction and quality checks were applied as in Arnqvist et al. (2015). The stratification was evaluated by means of
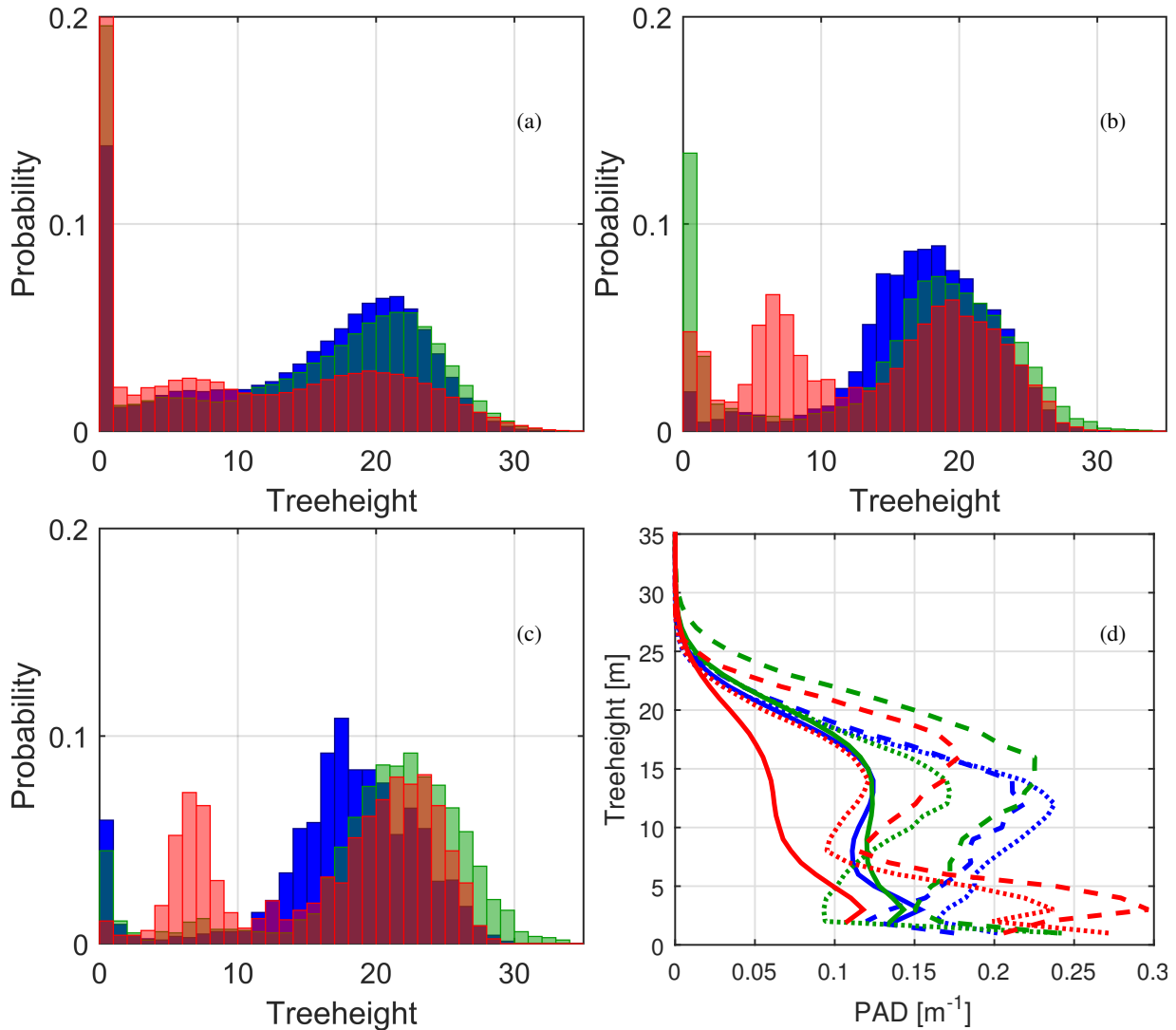
Figure 2. (a), (b) and (c) Distribution of tree heights in the three sectors within radius (a) 10 km, (b) 2 km and (c) 1 km. The colours indicate sectors $100°$ blue, $240°$ green and $290°$ red. (c), average PAD profiles from within 10 km as full lines, 2 km as dotted lines and within 1 km as dashed lines. Colouring as in the histograms.

$(z - d)/L$, where z is the height, d is the displacement height and L, the Obukhov length, was determined as

$$L = -\frac{u_*^3 T}{\kappa g \overline{w't'}},\tag{1}$$

where $u' = u - \bar{u}$, $w' = w - \bar{w}$, $u_* = (\overline{u'w'}^2 + \overline{v'w'})^{(1/4)}$, the friction velocity, $\kappa = 0.4$ is the von Kármán constant, $g = 9.81$ ms^{-2}, is the gravitational acceleration and $t' = t - \bar{t}$, is the instantaneous temperature fluctuation. To select only neutral

5 conditions $(z - d)/L$ was required to be between -0.1 and 0.07 at all heights. The limits where selected based on the shape of the ϕ-function for momentum (Högström, 1996) and allows for roughly a ± 35 % variation in the wind gradient given a certain u_* value. In addition, the 98 m wind speed was required to be between 7 and 8 ms^{-1} and the conditions quasi stationary, as defined by that the wind speed was allowed to vary maximum 10% between adjacent 10-min segments and the wind direction was allowed to vary maximum 10° between adjacent 30-min segments. After applying all the conditions and quality controlling

10 the data there remained 9, 13 and 9 30-min segments in the sectors 100°, 240° and 290° respectively.

4 Modelling

The models that participated in the benchmark where all CFD models using a RANS or LES methodology. The modelling has been performed by partners within the NEWA project. Table 1 shows an overview of models used by the respective partner. Some of the models include a full topography and PAD description. All of the models use a drag formulation to simulate the

15 forest, with a drag coefficient of 0.2 (except Meteodyn which uses another drag formulation, please see Section 4.2.2). In the following section more description about each model setup is given.

4.1 General CFD Modelling

Computational modelling of the fluid flow employs a simplified version of the Navier-Stokes equations, due to the impracticality of resolving every temporal and spatial scale. The Reynolds-Averaged Navier-Stokes (RANS) equations make use of

20 the Reynolds decomposition to divide the velocity field into the time averaged velocity and the velocity fluctuation around the mean, $u_i = \langle u_i \rangle + u_i'$. This yields a momentum equation for the mean flow where the effect of the turbulent motions is represented via the Reynolds stresses $\langle u_i' u_j' \rangle$, requiring a model to represent their effect on the average field. Most approaches (known as turbulence viscosity models) employ the Boussinesq approximation where the Reynolds stresses are parameterized in function of an eddy viscosity ν_t and a rate of strain tensor, which assumes that the turbulence fluxes are proportional to the

25 mean velocity gradient. This yields,

$$\frac{\partial \langle u_i \rangle}{\partial t} + \frac{\partial \langle u_i \rangle \langle u_j \rangle}{\partial x_j} = -\frac{1}{\rho}\frac{\partial \langle p \rangle}{\partial x_i} + \frac{\partial}{\partial x_j}\left[(\nu + \nu_t)\left(\frac{\partial \langle u_i \rangle}{\partial x_j} + \frac{\partial \langle u_j \rangle}{\partial x_i}\right)\right] + f_c \epsilon_{ij3}\langle u_j \rangle + \langle f_i \rangle,\tag{2}$$

as the momentum equation, where f_i represents an external body force. The Coriolis force is included using the Coriolis parameter $f_c = 2\Omega \sin\lambda$, where Ω is the Earth's rotational velocity and λ the latitude of the wind farm. The eddy viscosity is modelled through the introduction of transport equations, such as in the frequently employed $k - \epsilon$ technique.

RANS modelling supposes that the effect of all range of fluctuations on the mean flow can be accounted for by the models. Conversely, in the Large-Eddy Simulations (LES) approach the energy-containing flow structures are fully resolved, whereas only the effect of the smaller fluctuations is modelled. This is achieved through the decomposition of the velocity field into filtered (or resolved) and residual (or subgrid scale, SGS) components, $u_i = \overline{u}_i + u_{\text{SGS}}$. Although various types of filters exist, a

5 very common method in wind research is to associate a filter width to the grid spacing. The application of this decomposition on the Navier-Stokes equations leads to the apparition of the SGS stress tensor $\tau_{ij}^{\text{SGS}} \equiv -\rho(\overline{u_i u_j} - \overline{u}_i \overline{u}_j)$, that needs to be modelled. As in RANS, the prevalent strategy is to apply the Boussinesq approximation to introduce a subgrid viscosity ν_{SGS} to derive the LES momentum equation,

$$\frac{\partial \overline{u}_i}{\partial t} + \frac{\partial \overline{u}_i \overline{u}_j}{\partial x_j} = -\frac{1}{\rho}\frac{\partial \overline{p_m}}{\partial x_i} + \frac{\partial}{\partial x_j}\left[(\nu + \nu_{\text{SGS}})\left(\frac{\partial \overline{u}_i}{\partial x_j} + \frac{\partial \overline{u}_j}{\partial x_i}\right)\right] + f_c\epsilon_{ij3}\overline{u}_j + f_i, \tag{3}$$

10 where p_m denotes the modified pressure, which includes the isotropic part of the SGS stress tensor. The simplest approaches to calculate ν_{SGS} (and amongst the most commonly employed in wind research), make use of the resolved scales.

Table 1. Overview of used models and model family. [1] PALM used mean values of the ALS derived PAD combined with flat terrain

	Solver	RANS	LES	ALS input	Closure/SGS	Marker
Meteodyn	Meteodyn WT	x			$k - l$	*
EllipSys3D hi res 1	EllipSys3D	x		x	$k - \epsilon$	◁
EllipSys3D hi res 2	EllipSys3D	x		x	$k - \epsilon$	△
EllipSys3D low res 1	EllipSys3D	x		x	$k - \epsilon$	▷
EllipSys3D low res 2	EllipSys3D	x		x	$k - \epsilon$	▽
CFDWind	OpenFOAM	x		x	$k - \epsilon$	□
UUCGWind	OpenFOAM		x	x	k_{SGS}	○
Alya	Alya	x		x	$k - \epsilon$	+
PALM spatial average	PALM		x	x[1]	Deardorff-Smagorinsky	○
PALM vertical column	PALM		x	x[1]	Deardorff-Smagorinsky	◇

4.2 RANS

In the present work, the RANS models use one or two equations turbulence models. The two equations turbulence closure model used in the present work is a classical $k - \varepsilon$ model (Launder and Spalding (1974)), where transport equations for the

15 turbulent kinetic energy k and its dissipation rate ε:

$$\frac{\partial k}{\partial t} + \frac{\partial}{\partial x_j}(\langle u_j \rangle k) - \frac{\partial}{\partial x_j}\left(\left(\nu + \frac{\nu_t}{\sigma_k}\right)\frac{\partial k}{\partial x_j}\right) = \nu_t \frac{\partial \langle u_i \rangle}{\partial x_j}\left(\frac{\partial \langle u_i \rangle}{\partial x_j} + \frac{\partial \langle u_j \rangle}{\partial x_i}\right) - \varepsilon + S_k \tag{4}$$

$$\frac{\partial \varepsilon}{\partial t} + \frac{\partial}{\partial x_j}(\langle u_j \rangle \varepsilon) - \frac{\partial}{\partial x_j}\left(\left(\nu + \frac{\nu_t}{\sigma_\varepsilon}\right)\frac{\partial \varepsilon}{\partial x_j}\right) = C_{\varepsilon 1}\frac{\varepsilon}{k}\nu_t\frac{\partial \langle u_i \rangle}{\partial x_j}\left(\frac{\partial \langle u_i \rangle}{\partial x_j} + \frac{\partial \langle u_j \rangle}{\partial x_i}\right) - C_{\varepsilon 2}\frac{\varepsilon^2}{k} + S_\varepsilon \tag{5}$$

are solved.

$C_{\varepsilon_1}, C_{\varepsilon_2}, \sigma_k, \sigma_\varepsilon$ are modelling constants and S_k, S_ε are the source/sink terms representing the drag based energy loss in the canopy. The eddy viscosity is determined from:

$$\nu_t = C_\mu \frac{k^2}{\varepsilon} \qquad (6)$$

5   where C_μ is another modelling constant.

Following Sogachev and Panferov (2006) the source/sink canopy terms are parametrised as:

$$S_k = 0 \qquad (7)$$

$$S_\varepsilon = 12 \left(C_{\varepsilon_2} - C_{\varepsilon_1} \right) C_\mu^{\frac{1}{2}} C_d \, a \mid \langle \mathbf{u} \rangle \, \varepsilon \qquad (8)$$

where C_d is a drag coefficient and a is a frontal area density.

10   The length scale in the standard $k - \varepsilon$ model is not bound and grows indefinitely with height. In order to adjust the model to ABL relevant flow cases, a correction suggested by Apsley and Castro (1997) is applied, where the $C_{\varepsilon_1}^*$ constant is (re)defined in a following manner:

$$C_{\varepsilon_1}^* = C_{\varepsilon_1} + (C_{\varepsilon_2} - C_{\varepsilon_1}) \frac{l}{l_{max}}, \qquad (9)$$

with the mixing length l defined by:

15   $$l = C_\mu^{\frac{3}{4}} \frac{k^{\frac{3}{2}}}{\varepsilon} \qquad (10)$$

The limiting maximum length scale l_{max} is determined based on the relationship proposed by Blackadar (1962):

$$l_{max} = \frac{0.00027 \, G}{f_c} \qquad (11)$$

where G is the geostrophic wind and f_c the Coriolis parameter.

The two equation methodology explained above is used by Ellipsys3D, CFDWind and Alya. In the case of Meteodyn, a
20   one equation RANS turbulence model k-l_m is instead used Delaunay (2007). This methodology consists of solving the TKE equation (4), replacing ε in terms of k and a parametrized mixing length l_m. Thus $\varepsilon = \varepsilon(k, l_m)$.

Furthermore, assuming the canopy elements exert a drag force on the flow, effects of the plant drag inside the canopy on the main flow are parametrized, presuming the form drag dominance, in the momentum equations eq. (2) as:

$$\langle f_i \rangle = \langle f_{D,i} \rangle = -C_d \, a \mid \langle \mathbf{u} \rangle \mid \langle u_i \rangle \qquad (12)$$

Table 2. Model constants

	Standard $k-\epsilon$	Modified $k-\epsilon$	Modified2 $k-\epsilon$	$k-l$	LES
$C_{\epsilon 1}$	1.52	1.176	1.13	0	-
$C_{\epsilon 2}$	1.833	1.920	1.9	0	-
C_μ	0.09	0.033	0.0256	0	-
C_d	0.2	0.2	0.2	-	0.2
$C_d^* = C_d/A$	-	-	-	0.005	-
$\sigma_k 1$	1.0	1.0	0.7407	0	-
$\sigma_{\epsilon 1}$	1.7039	1.238	1.2987	0	-

4.2.1 Meteodyn

4.2.2 Model description

Meteodyn WT is a commercial site assessment software that models the surface boundary layer (no Coriolis force included) using the RANS equations coupled with a 1-equation turbulence model and wall functions based on Monin-Obukhov theory

5 Delaunay (2007). Meteodyn WT version 5.2.1 was used in the present investigation.

The turbulence is parametrized using the 1-equation k-l_m turbulence model Delaunay (2013); Hurley (1997) This turbulence closure scheme uses a prognostic equation for the turbulent kinetic energy and a mixing length approach for estimating the turbulent diffusion.

The forest model in Meteodyn is based on a mean flow model, which treats the forest as a porous media Costa. (2007),

10 similar to what is used in other commercial solvers like Windsim Crasto (2006). A volumetric sink term is introduced in the momentum equations for all cells lying inside or partially covering the forest volume. The volumetric force depends on the drag coefficient C_d, which is a function of the forest density. In the Meteodyn simulations presented in this paper we used a value of $C_d^* = 0.005$.

In Meteodyn the canopy height h for each cell is directly derived from the local roughness using the relation $h = Cz_0$, with

15 C an adjustable constant usually set to 20 and z_0 the roughness length at the cell surface. Cells with roughnesses higher than 0.8 cm are considered forest in the domain. Meteodyn can only handle roughness information provided in the .map format (contour lines information as in the WASP software was). For this reason, it was not possible to use the detailed plant area density information provided in the cloud of points for the Ryningsnäs benchmark. The Meteodyn simulations presented here use roughness maps derived from SRTM data obtained using windPRO win.

20 Two versions of the forest model are available in Meteodyn, which differ in the computation of the mixing length in the 1-equation turbulence model, named as robust and dissipative in the Meteodyn documentation. The dissipative forest model is used in the Meteodyn simulations presented in this investigation. In this model a 15 m extra high dissipation zone is used above the forest.

4.2.3 Numerical setup

A cartesian structured mesh on a square domain with dimensions 13.5×13.5 km^2 and 2.9 km height. The mesh is refined around the met mast location, with a grid stretching factor of 1.1 in the horizontal and 1.2 in the vertical direction. The final mesh has 224,000 cells. On the vertical direction the lines are always orthogonal to the topography surface.

5   Monin-Obukhov inlet profiles for velocity are defined at the inlet of the domain, as well as a constant turbulent kinetic energy Richards and Hoxey. (1993). The sides of the domain are defined as symmetry planes. The top and outlet sides of the domain are set with pressure outflow boundary conditions. At the domain surface wall functions are used, based on the local roughness of the cell and thermal stability classes.

4.2.4 EllipSys3D

10 ### 4.2.5 Model description

EllipSys3D is a CFD solver designed for various wind engineering applications – e.g. atmospheric boundary layer flows, turbine rotor computations etc. It is a multi block finite volume solver of the incompressible Navier-Stokes equations in the general curvlinear coordinates. It uses collocated variable arrangement, employing revised Rhie/Chow interpolation technique in order to avoid the odd-even pressure coupling. The pressure velocity coupling in the present study was based on the SIMPLE

15 algorithm. Furthermore, the code is designed based on a non-overlapping domain decomposition technique, which combined with its MPI parallelization, enables it to highly efficiently run on distributed/shared memory HPC systems.

The standard and modified model constants according to Table 2 are used in the EllipSys3D setup in the present work. The geostrophic wind chosen is $G = 13$ ms^{-1}, giving the maximum length scale of $l_{max} = 28.71$ m. A 1D-precursor computation has been conducted in order to obtain the suitable inlet profiles, applied at all inlet boundaries.

20   To be able to model the effects of surface roughness on the mean flow and avoid resolving the laminar sub-layer, wall-functions as boundary conditions at wall surface boundaries are typically applied. In EllipSys3D, the wall boundary is placed on the top of the roughness elements, allowing that large near surface velocity gradients can be resolved using shallow (high aspect ratio) computational cells. The wall shear stress is accordingly used to specify the wall boundary conditions for momentum- and ε- equations, while a von Neumann boundary condition is set for k - for detailed description see (Cavar et al. (2016)) .

25 A uniform roughness of 0.1 m is applied on the whole wall surface. The laser scan map provided for the present benchmark extending over a 52.5 km x 52.5 km zone centred at the Rygningsäs site location, basically covering the whole wall surface area in the present study, was also fully incorporated into the EllipSys3D computations.

4.2.6 Numerical setup

The computational domain is a circular grid with a radius of 17 km, centred at the Rygningsnäs met mast location. The inner

30 zone surrounding the site has a quadratic form. It is based on equally spaced grid points and covers a zone of 5 km x 5 km. The inner zone domain fully resolves the underlying topography, while the topography in the outer (buffer) zone is gradually

smoothed towards the outer boundary. The same computational grid is used for all three investigated cases (flow directions), only the inflow and outflow boundaries on the grid circumference were adjusted for the each single run accordingly. Two grid sizes are considered, one using 512 x 512 grid points in the inner zone and 128 points in the outer (buffer) zone and the other one using 128 x 128 grid points in the inner zone and 64 points in the outer zone. The 3D grid was constructed by using an

5   EllipSys3D default hyperbolic grid generator. 192 points were used in the vertical direction, with the first cell located at 1 cm above the terrain. The vertical hyperbolic mesh growth was controlled, so the zone up to a 50 m height had cells not higher then 1 m. The top boundary was located at a 9 km height. The considered grids had approximately 100 million grid points (3072 blocks of 32^3) in the 10 m resolution run and approximately 9.5 million grid points (288 blocks of 32^3) in the 50 m resolution run.

10   **4.2.7   Alya**

4.2.8   Model description

The RANS model has been implemented in Alya, a high performance computing (HPC) code developed at BSC able to run large-scale applications. The code was recently tested on $100,000$ processors with a parallel efficiency above 90% et al (2016).

The Navier-Stokes (2) and turbulence equations (4)-(5) are discretisized using a stabilised finite element method using equal

15   interpolation for all the unknowns. As stabilisation scheme we used the Algebraical Subgrid Scale method (ASGS) Codina (1998) extended for nonlinear equations Avila et al. (2015), which gives stability to convection and Coriolis dominating terms in the momentum equation and to convection and reactive terms in the turbulence equations, removing spurious oscillations. The ASGS stabilisation method gives also stability to pressure, allowing equal interpolation spaces for pressure and velocity. The velocity-pressure problem is decoupled using an Orthomin solver Houzeaux et al. (2011) that converges to the monolithic

20   scheme.

A robust finite element scheme written in block-triangular form Codina and Soto (1999) is obtained for the k-ε equations (4)-(5). In order to avoid instabilities and numerical convergence issues k and ε unknowns are not allowed to drop below a predefined limit by applying a clipping. In addition, the innermost iterative loops of the k and ε equations (4)-(5) are linearized using a Newton-Raphson scheme for the quadratic terms, considering ν_t and P_k constants within the innermost loops.

25   Once the algebraical system of equations are obtained, a Deflated Conjugate Gradient Lohner et al. (2011) solver with a linelet pre-conditioner Soto et al. (2003) is used to solve the pressure, and a Generalized Minimizing Residual (GMRES) solver is used for the velocity and turbulence unknowns.

4.2.9   Numerical setup

The Ryningsnäs problem was solved using a cylindrical Mesh with a radius of 20 km. The mesh is centred in the mast.

30   Surrounding the mast the mesh resolution is 10 m over a 4 km $\times 4$ km horizontal square. Farther from the mast the horizontal mesh size grows until 500 m horizontal element length. The vertical resolution starts with a 0.5 m element length close to the wall, being of 1.2 meters inside the forest. The computational domain has a vertical extension of 2000 m.

The inflow boundary conditions are defined from a precursor simulation over flat and homogeneous terrain (i.e. single column model 1D). The obtained fields are used also as initial condition. Zero traction is imposed over the outflow boundaries. No velocity penetration and zero tangential stress are imposed over the top boundary.

Three different geostrophic velocities were set to the three different wind directions to match the desired velocity at mast. The geostrophic velocities were set to 12.7 m/s, 13.2 m/s and 12.7 m/s for the wind directions of 100, 240 and 290 degrees respectively.

4.2.10 CFDWind

4.2.11 Model description

CFDWind is a modelling framework developed in CENER on top of the open-source CFD platform OpenFOAM Weller et al. (1998) version 2.4.0 ope (2015). The model is designed for the simulation of atmospheric boundary layer flows through the solution of the incompressible RANS equations in which turbulence closure is achieved by the eddy-viscosity theory and a modified version of the $k - \varepsilon$ closure scheme Apsley and Castro (1997) described in the previous section.

As only neutral atmospheric stability was considered, the flow is assumed stationary so the SIMPLE algorithm is employed to solve the pressure-velocity coupling whilst 2nd-order upwind schemes are used for the discretization of both velocity and turbulence convective terms.

The Coriolis apparent force is added explicitly to the momentum equation together with the horizontal pressure gradient that drives the system which is derived from the hydrostatic relation for stationary cases.

The perturbations induced by forests are modelled by adding drag and source/sink terms in the momentum and turbulence-closure equations, respectively, as proposed by Sogachev and Panferov (2006). Table 2 (Modified2 $k - \epsilon$) shows the drag and closure-model constants employed for the simulations. Rather than tuned, these values follow the set employed by Detering and Etling (1985) which are derived from the experiments carried out in Panofsky et al. (1977).

Despite it is expected that wind flow is dominated by the effects of forest features near the surface, z_0-based wall functions are implemented as boundary conditions at the ground assuming wall bounded flow. That is, the applied horizontal kinematic shear stress is set via an effective eddy-viscosity ν_t^{wall} which together with the dissipation rate and production term of the turbulent kinetic energy equation are obtained with the local velocity scale u_*^{wall} computed from values of velocity and turbulent kinetic energy of the cells adjacent to the ground (see Chávez-Arroyo et al. (2014) for more details).

Similar to EllipSys3D, the wall functions consider that the computational grid is placed on top of the roughness elements so that restrictions related to the height of the cells adjacent to the ground and z_0 are avoided and high aspect ratio cells can be used. Outlet conditions are specified at the sides and at slip (only tangencial velocity and no-gradient) conditions are prescribed at top of the domain.

4.2.12 Numerical setup

The numerical grid was created with the meshing software WindMesh. The tool has been developed jointly by BSC and CENER for the automatic and fast generation of grids over terrain. There are currently two different versions further developed by each institution: BSC-WindMesh Gargallo-Peiró et al. (2015) which was employed in the simulations of the Alya model, and the CENER-WindMeshPaweł and Roberto (2017) version which was used for the generation of the grids for the UUCG and CFDWind runs.

CENER-WindMesh creates structured terrain-following grids optimizing parameters such as orthogonality and skewness by applying filters to the 2D (ground) mesh, and elliptic smoothing techniques for the final 3D mesh. The mesh is designed so that terrain is smoothed far from the area of interest whereas towards the central zone the cells are refined to the maximum resolution established. Only real topography is considered for the grid generation in the center. The "transition" zone between boundaries and the central zone is a progressive blend between the real terrain and flat boundaries.

Similarly to previous approaches, a precursor run is conducted prior to the full-terrain simulation (successor) in order to create the equilibrium profiles that serve as inlet conditions. Precursor simulations consist on flat domains with periodic boundary conditions on the sides with the top and wall-treatment mentioned above. The PAD is set to a constant value of 19 m^{2}m^{-3} with values of roughness length and forest height of 0.72 m and 14 m, respectively. For the successor runs, the heterogeneous roughness values are created based on the canopy height map, H, using the simple relation of $z_0 = H/20$.

The value of geostrophic wind is chosen so that the velocity magnitude obtained in the simulations is approximately 10 ms^{-1} at 100 m at the position of the mast for each of the three flow cases. The values are 14.66, 15 and 15 ms^{-1}, resulting in maximum length scales of $l_{max} = 32.2$, $l_{max} = 33$ and $l_{max} = 33$ m for the inflow directions of 100, 240 and 290 degrees respectively.

The computational domain is squared-shaped and covers an extension of 18 km $\times$18 km $\times$3 km centered in the Ryningsnäs tower. From that, only a 12 km $\times$12 km region considers real topography in which PAD and z_0 data are interpolated from the input canopy information. The rest of the domain is set as a flat, buffer area with the same PAD, z_0 and H of the precursor simulation. For each flow case, the mesh is rotated in order to align the wind direction with the normal vector of the inlet patch at 100 m above ground. The meshes consist in 20×10^6 cells with 60 vertical levels. First cell height is set to 1 m and then grows with a geometric function with a constant growth rate of 1.08.

4.3 LES

4.3.1 UUCG-Wind

4.3.2 Model description

The computations by UUCG were carried using the OpenFOAM platform, version 3.0.1. A neutrally-stable wind flow is computed with LES coupled with a SGS model (Yoshizawa and Horiuti, 1985; Yoshizawa, 1986) were ν_{SGS} is estimated from the subgrid turbulence kinetic energy k_{SGS} which is in turn computed from a transport equation. The flow computation is then

simulated with a model implementation based on modifications to the solver `pisoFoam` and the SGS model `kEqn` available in OpenFOAM. Accordingly, the PISO algorithm is employed for the solution of the pressure-velocity equations. A backward interpolation scheme is applied in the solution of the transient term and central differencing for the remining terms.

It is assumed that the forest acts as a porous surface exerting a drag on the flow. This is represented in the simulation with the introduction of a source term in the LES momentum equation (eq. 2):

$$f_{D,i} = -C_D a |\overline{\boldsymbol{u}}| \overline{u}_i \tag{13}$$

where C_D is the forest drag coefficient, a is the frontal-area-density (assumed here equal to the PAD). This approach has been successfully used in wind computations over forest with LES, e.g. by Nebenführ (2015) and Boudreault (2015). The employed value of $C_D = 0.2$ throughout the domain is taken from the latter. While the effect of the forest in eq. (13) is applied over the resolved part of the velocity field, the dissipative effect of TKE caused by the forest is included within the subgrid scales by adding the term

$$\varepsilon_{\text{SGS}} = -\frac{8}{3} C_D a |\overline{\boldsymbol{u}}| k \tag{14}$$

to the transport equation of k_{SGS}.

A wall model is also used to account for the roughness of the ground, although it is expected that its influence on the wind flow will be much smaller in comparison to the forest. To this aim, the wall model implementation available in the OpenFOAM libraries of SOWFA (Churchfield et al., 2014) was employed. Hereby, the velocity deficit due to the interaction with the ground is introduced indirectly, by means of applying a surface stress. For this, the model of Schumann (1975) is used, where the non-zero components of the stress tensor at the surface are computed as a function of the friction velocity, which in turn is calculated from the logarithmic law with a local time-average for the horizontal velocity. Only the modules corresponding to the modelling of the surface stress are used from SOWFA, importing these from OpenFOAM 2.x into the version used for the simulations.

4.3.3 Numerical setup

The computational domain consists of a box of dimensions $L_x \times L_y \times L_z = 32 \, \text{km} \times 20 \, \text{km} \times \sim 1.2 \, \text{km}$ (L_z varies due to the differences in terrain elevation for each wind direction), where axes describe directions aligned with the streamwise, spanwise and vertical directions of the domain. The met mast is located at $20 \, \text{km}$ in the longitudinal direction, in the mid-spanwise crossing. The mesh is created using the same grid generator as the one employed for CFDWind in section 4.2.10, producing a mesh with a varying ground elevation from the terrain file with a resolution of $10 \, \text{m} \times 10 \, \text{m}$. Therefore, the grid consists of zones in the horizontal plane: a farm zone ($L_x \times L_y = 20 \, \text{km} \times 12 \, \text{km}$, met mast at $14 \, \text{km}$) at the interior which is then successively surrounded by a transition zone and a buffer zone. The two outermost regions can be described as rectangular edges with a width in the longitudinal and spanwise directions of 3 km and 2.5 km for the transition zone and 3 km and 1.5 km for the buffer zone. The arrangement of the grid in the horizontal plane is uniform in the farm and buffer regions, while the cells stretch in the transition zone, changing their size from that of the farm to the one of the buffer zones. The terrain becomes

flat at the buffer edges until, at the outermost boundary (with a width of 500 m), the elevation is equal in all sides with a value of 63.06 m (100 degrees), 163.25 m (240 degrees) and 137.76 m (290 degrees). The horizontal cell resolution is 25 m for the farm and 250 m in the buffer regions. The height of the first cell at the location of the met mast is approximately 5 m while the size increases vertically with a growth rate of ~ 1.05. The domain height as well as the number of cells in the vertical direction

5 in every case is $L_z = 1.172$ km and $N_z = 84$ cells for 100 degrees, $L_z = 1.305$ km and $N_z = 86$ cells for 240 degrees as well as $L_z = 1.267$ km and $N_z = 85$ cells for 290 degrees.

The longitudinal axis of the domain is aligned with the wind direction for each case, so the inlet is perpendicular to the inflow. All lateral boundaries are set to periodic boundary conditions. Hence, the inlet flow is recycled from the outlet. The flow is driven by a uniform pressure gradient, following the procedure described by Bechmann (2006) which also comprises

10 the introduction of Coriolis forcing (assuming a latitude of 57 degrees). In this manner, the pressure gradient is calculated for the desired geostrophic wind, which is set as to yield the desired wind velocity at 98 m for each case. The complete height of ABL is simulated to avoid the parametrization of the components of the shear stress, as they become negligible at this altitude. The ground surface is set to a wall with a uniform roughness of $z_0 = 0.03$ m, while the PAD for the cells covering the tree area is extracted (by linear interpolation) from the file of $10\,\text{m} \times 10\,\text{m}$ resolution, using the same method as for CFDWind in section

15 4.2.10. For each wind direction, simulations are run during about 400×10^3 s to develop the flow and achieve convergence of second-order statistics. Results are obtained from values averaged during subsequent computations lasting 20×10^3 s with $\Delta t = 0.296$ s, yielding a maximum Courant-Friedrichs-Lewy number of CFL ≈ 0.6 over the whole domain.

4.3.4 PALM

4.3.5 Model description

20 PALM is a massively parallelized LES model designed for studies of the atmospheric and oceanic boundary layer. It is an open source code (PAL) and has been applied to the simulation of a variety of atmospheric boundary layer studies in the past 20 years. PALM solves the filtered, incompressible, non-hydrostatic Navier-Stokes equations under the Boussinesq approximation on an equidistant Cartesian grid. The sub-grid scale turbulence is parameterized by a 1.5th order closure after Deardorff (1980). Further details on the numerics and physics of PALM can be found in Maronga et al. (2015).

25 The forest effect is modelled by adding a sink term to the momentum equation following Shaw and Schumann (1992) and Watanabe (2004). Furthermore a sink term is added to the prognostic equation for the SGS TKE according to Shaw and Schumann (1992) to ensure a rapid breakdown of turbulence in the canopy. A source term is added to the temperature equation allowing to prescribe a heat flux at the canopy top to account for the effect of incoming solar radiation. See Kanani et al. (2014) for equations and further details of the canopy model. A forest canopy can be prescribed by specifying the tree height and a

30 vertical PAD profile. The PAD profile can be prescribed by using a beta probability density function (parameters α, β and leaf area index) or by specifying PAD values at discrete levels and doing a piecewise linear reconstruction. The latter approach has been used for the benchmark simulations. As per default, only a single PAD profile and tree height can be specified and

hence, only a homogeneous forest can be simulated. Simulating a heterogeneous forest would have required significant code development which has not been feasible in the scope of the benchmark.

4.3.6 Numerical setup

The benchmark simulations use a model domain of 2304 m x 1152 m x 1867 m with a grid spacing of 4 m. A homogeneous

5 forest canopy is prescribed by setting periodic horizontal boundary conditions and using averaged PAD profiles where each of the three sectors has been averaged over the innermost 2 km. A conventionally neutral atmospheric boundary is simulated by prescribing a constant potential temperature up to a height of 500 m capped by a stable layer with a gradient of 1 K / 100 m. Coriolis force is considered assuming a latitude of 57 degrees North). The roughness length is set to 0.1 m. A geostrophic wind speed of $u_g = 13.0$ ms^{-1} and $v_g = -9.3$ ms^{-1} had to be prescribed to achieve a mean wind along x direction in 100

10 m height of about 7.4 ms^{-1} as demanded by the benchmark specification. The simulations have been run for 10 h to reach a steady state. The results have been averaged over the entire horizontal model domain and over the last 30 min of the simulation. Additionally, a vertical point profile at the centre of the domain, averaged over 2 h, has been provided.

4.4 Numerical set up overview

To summarise, four different RANS codes and two different LES codes are included in the study. Forest modelling is basically

15 done in the same way in all codes apart from Meteodyn. All models apart form PALM uses heterogeneous forest, but Meteodyn is based on a different surface data set. Domain sizes are similar apart from PALM which uses a significantly smaller domain, but since PALM have homogeneous forest with re-circulation the domain size is directly comparable. A summary of some key modelling properties is found in Table 3. The numerical challenge stretch from the use of a commercial code to state-of-the-art research codes using up to about 40 million cells, modelling of 20 000 physical second and the use of approximately 20 000

20 CPU hours.

Table 3. Numerical setup. Cell size refers to the horizontal grid size in the inner domain.

Model	Cell Size [m]	$a \times b \times c$ [km]	G[m/s]	Mesh generator
Meteodyn	15	$13.5 \times 13.5 \times 2.9$		
EllipSys3D hi res 1	9.8	34 (diameter) $\times 9$	13	
EllipSys3D hi res 2	9.8	34 (diameter) $\times 9$	13	
EllipSys3D low res 1	39.1	34 (diameter) $\times 9$	13	
EllipSys3D low res 2	39.1	34 (diameter) $\times 9$	13	
Alya	10	$20 \times 20 \times 2$	12.7, 13.2, 17.7	WindMeshGargallo-Peiró et al. (2015)
OpenFoam CFDWind	12	$18 \times 18 \times 3$	14.6,15,15	WindMesh Paweł and Roberto (2017)
OpenFOAM UUCG	25	$32 \times 20 \times 1.2$	11.5, 12.5, 11.4	WindMesh Paweł and Roberto (2017)
PALM	4	$2.3 \times 1.2 \times 1.9$	16.0	
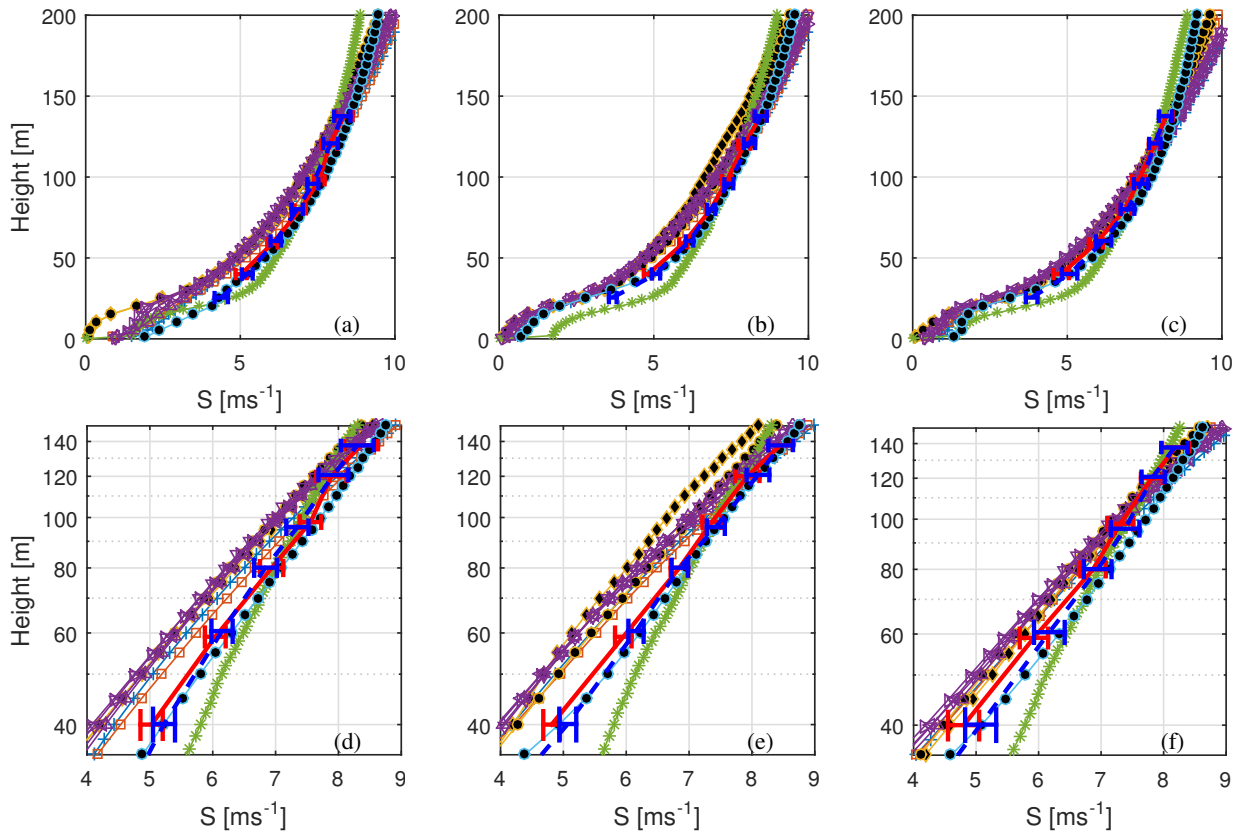
Figure 3. Wind speed profiles.The blue dashed line show the average from the cups, the red full line show the average from the sonics. Error bars indicate the 95 % confidence level for the mean value. The various other markers indicate simulated wind speeds. Please see table 1 for the marker representations. LES models have been given black filling in order to increase readability. (a) and (d) shows results from 100 °, (b) and (e) from 240 ° and (c) and (f) from 290 °.

5   Results

One main purpose of RANS and LES modelling within the wind energy community is to extrapolate tower measurements vertically and spatially. In the following section, first the vertical extrapolation (vertical profiles) and then the horizontal extrapolation (planes) is reported.

5   ### 5.1   Vertical profiles

Crucial to the power production is the wind speed, turbulence level and wind veer. These three quantities, in the form of wind mean speed $S = \sqrt{U^2 + V^2}$, mean turbulence kinetic energy $\mathrm{TKE} = 0.5(u^2 + v^2 + w^2)$ and mean wind direction is evaluated in figure 3, figure 6 and figure 5 respectively.
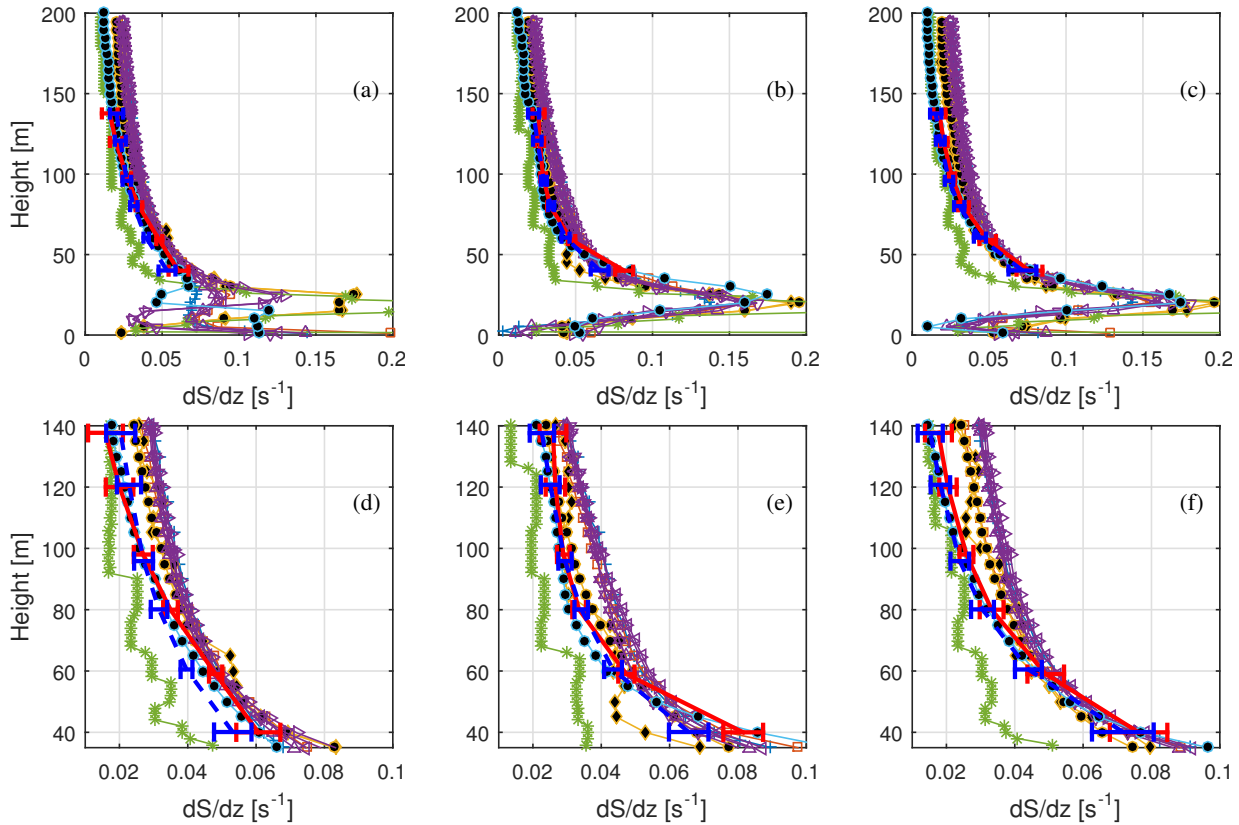
Figure 4. Wind speed gradient profiles. The lower three plots are zoomed in on the instrument heights to increase readability. The blue dashed line show the average from the cups, the red full line show the average from the sonics. Error bars indicate the 95 % confidence level for the mean value. The various other markers indicate simulated wind speeds. Please see table 1 for the marker representations. LES models have been given black filling in order to increase readability. (a) and (d) shows results from 100 °, (b) and (e) from 240 ° and (c) and (f) from 290 °.

Modelled and measured profiles are shown for the three different wind directions described in Section 3.2. As is apparent from studying Figure 3 most models actually show a slightly lower wind speed than the targeted 7.4 ms^{-1} at 100 m height. The wind profiles are also provided in logarithmic height coordinates and it is apparent that the measurements have a deeper log-linear region than most of the modelled curves.

5 Most models overestimates the wind speed gradient, reported in Figure 4. The overestimation increases with height and in the upper layers is close to a factor 2. The fact that most models have a lower 100 m wind speed compared to the target 7.4 ms^{-1} means that one has to be careful when interpreting how good the models are at estimating the wind speed gradient, but a 0.5 ms^{-1} difference in 100 m wind speed roughly means a 5×10^{-3} s^{-1} difference in wind speed gradient (assuming the difference is spread out over 100 m). As can be seen in Figure 4 the difference, for most models, is at least twice as large and

10 consistently over predicted by all RANS models except Meteodyn. Meteodyn is the only RANS not to use the PAD input and

thus it is difficult to know whether the smaller shear is due to the surface boundary condition or some other modelling aspect. In terms of shear one can see that OpenFoam UUCG stands out as the best performing model. The forest parameterization and PAD data were the same for that model as for the RANS models using PAD, so the difference in shear cannot be explained by difference in amount and placement of the surface drag elements. The main difference between OpenFoam CFDwind and

5   OpenFoam UUCG is that the latter is run in LES mode which seem to result in either better estimation of the boundary layer height or more realistic mixing of the velocity deficiencies, or both. The other LES model, PALM, did not run with the detailed PAD input, but did use averaged PAD profiles averaged with the innermost 2 km radius for each of the three directions. As seen in Figure 3 and 4 PALM does have lower shear compared to the RANS models, but it is unclear how much of that is due to the LES effect and how much is due to the constant PAD profile used. One interesting thing to notice is that while all

10   the models using the detailed PAD fields, as well as the measurements, have largest shear at 100 m in the 240° sector, PALM shows the largest shear in 290° at 100 m despite having much lower PAD in that direction. This is in line with analytical theory for homogeneous forests which predict a maximum of the roughness length at moderate PAD after which blocking effects lead to gradually lower roughness lengths with increasing PAI Jackson (1981). Most forests considered for wind energy have a substantial heterogeneity, though, and as can be seen in Figure 1b the lower average PAD within the innermost 10 km does

15   not come from areas with less dense forest, but rather from a large area *without* forest, over which the flow may be able adopt to a lower roughness environment.

In an earlier publication Arnqvist et al. (2015) it was shown that the wind turning with height, the veer, was considerable at rotor heights, especially in stable stratification. As can be seen in Figure 5 most models show a veer of 1-3 degrees between 50 and 150 m. This is about half of the veer from the measurements, but the kinking of the measured curves also indicate

20   the difficulty in measuring small deviations of the wind direction as wind load on the tower and booms as well as alignment accuracy all add to the uncertainty. The general shape of the wind direction profile in the Ekman layer however suggests that the models represent the relevant physics accurately apart form the Meteodyn model that has a strange behaviour of the the wind direction and does not seem to be coupled to the balance between Coriolis force, stress divergence and pressure gradient. Another very interesting point is that all the models using detailed PAD input show a reverse in the wind direction turning

25   centered between 20 and 60 m, placed lowest in 240° and highest in 100°. This reverse indicates that at this height pressure gradient is no longer important for driving the flow, being cancelled by strong the drag of the forest, and the main driving force is instead the flux divergence, similar to an ocean current.

Out of the three directions 290° stands out as the direction with the lowest overall mean PAD, as seen in Figure 2. The main contributor to the lower PAD average is however mainly low forest or lack of forest in the far upstream region which is

30   apparent from Figure 1 (b) where an area without forest is seen at around 7-12 km fetch in the 290° direction. It is likely this low roughness area that causes the TKE level to drop more quickly with height in 290° compared with the other directions (Figure 6). While all models seem to get the overall level of TKE approximately right only the LES version of OpenFoam captures the decrease of TKE with height for all three directions. The RANS models show much less variation between the different directions. Interestingly, the PALM LES shows almost no difference in TKE between the different directions even
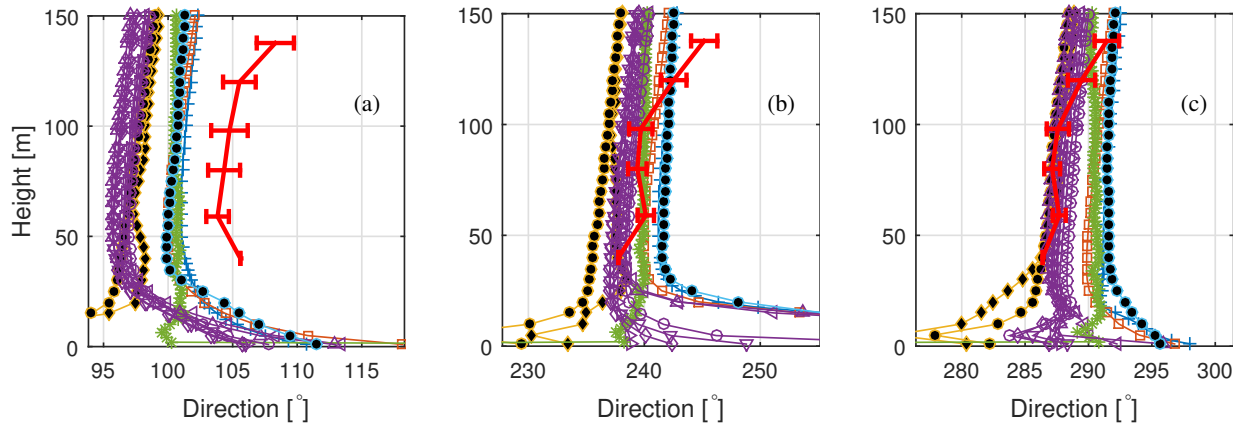
Figure 5. Wind direction profiles. The red full line shows the average from the sonics. Error bars indicate the 95 % confidence level for the difference between the wind direction at each height and direction at 40 m. The various other markers indicate simulated wind directions. Please see table 1 for the marker representations. LES models have been given black filling in order to increase readability. (a) shows results from 100 °, (b) from 240 ° and (c) from 290 °.
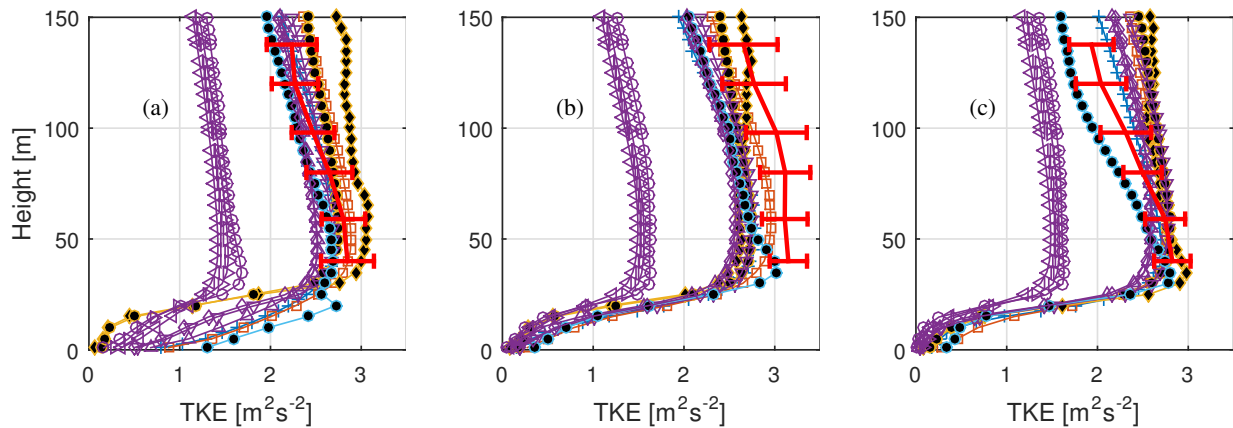
Figure 6. TKE profiles. The red full line shows the average from the sonics. Error bars indicate the 95 % confidence level for the mean value. The various other markers indicate simulated TKE levels. Please see table 1 for the marker representations. LES models have been given black filling in order to increase readability. (a) shows results from 100 °, (b) from 240 ° and (c) from 290 °.

though the average PAD is different in all three directions, see Figure 2 (d). It should be noted though, that the PALM wind speed at 100 m was lower in 240° which may explain why the turbulence level is not higher for that sector.

The purple lines in Figure 6 shows the different setups of EllipSys3D RANS, and while the effect of resolution does not seem to influence the results much (used values are found in Table 3), the choice of turbulence closure constants play a huge role (values found in Table 2). The use of standard $k - \epsilon$ values produce only about half of the TKE compared to the values tuned for atmospheric boundary layers despite the shear being virtually the same.

5.2 Horizontal planes
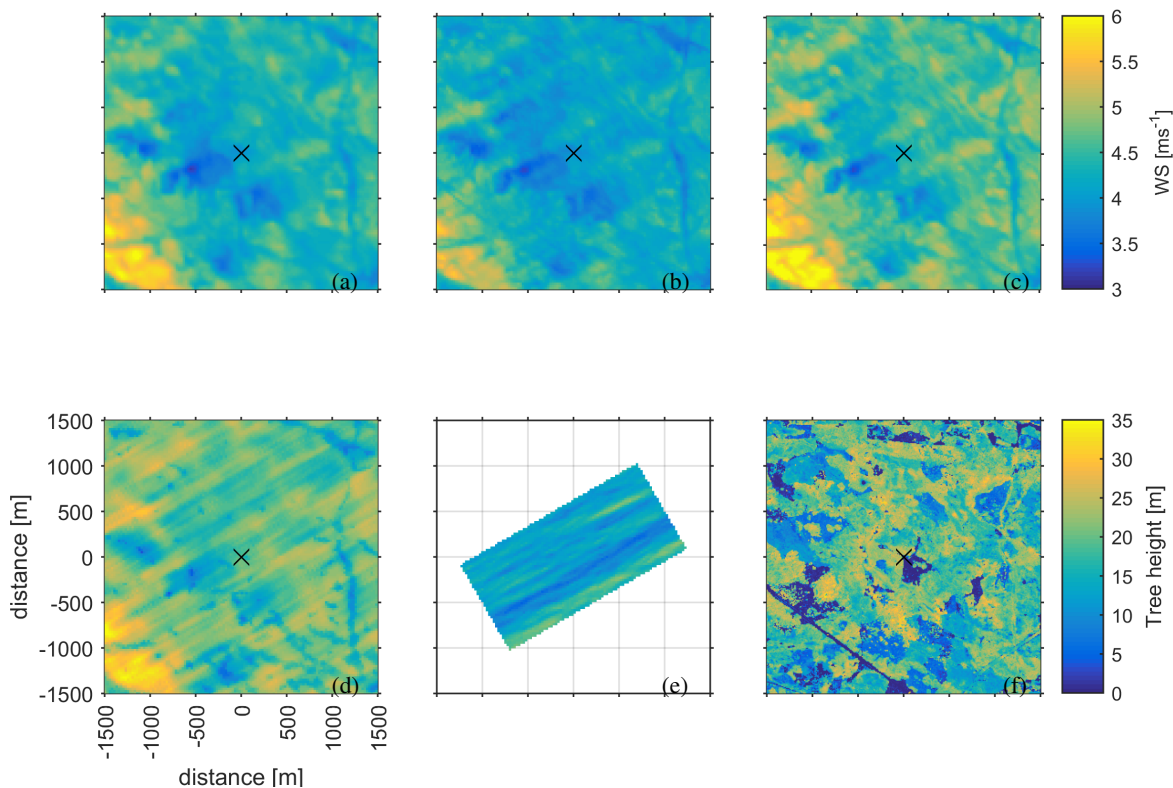
Figure 7. (a)-(e) Simulated wind speed at 40 m above the local ground height. (a) EllipSys3D hi res 1, (b) Alya, (c) OpenFoam CFDWind, (d) OpenFoam UUCG and (e) PALM. The size of the boxes is 3x3 km centered around the measurement tower (marked by an x). (f) The forest height.

In order to evaluate spatial differences the modellers where instructed to submit horizontal planes surrounding the measurement tower. Planes are shown here for 40 meter above the local elevation, Figure 7, and 140 m above the local elevation, Figure 8. Also displayed in the figures are tree height and terrain elevation. Although there is some correlation with tree height at 40 m, most of the correlation is with elevation, reflecting that the height is above local terrain and all models can be seen to have

wind fields with streamlines that are smoother than the terrain, which results in higher wind speed over high terrain and lower wind speed over low terrain. This feature is common for all models having varying terrain.
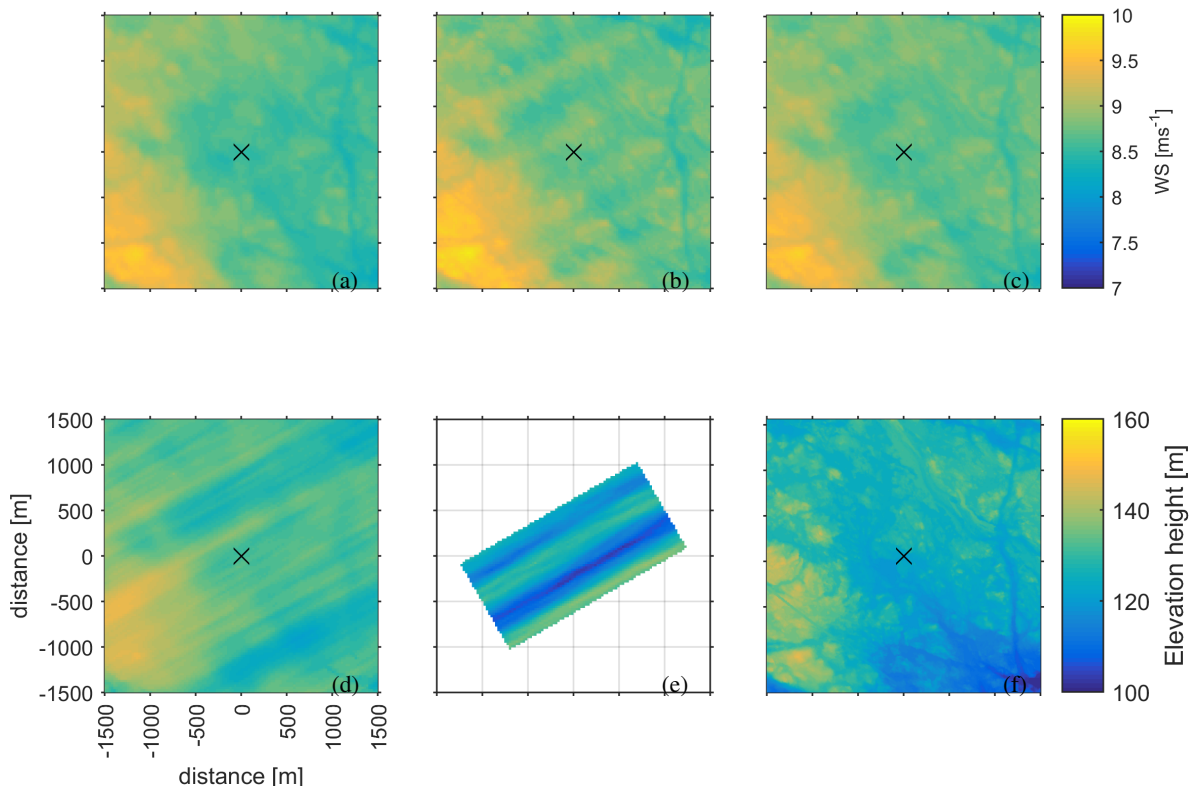
Figure 8. (a)-(e) Simulated wind speed at 140 m above the local ground height. (a) EllipSys3D hi res 1, (b) Alya, (c) OpenFoam CFDwind, (d) OpenFoam UUCG and (e) PALM The size of the boxes is 3x3 km centered around the measurement tower (marked by an x). (f) The elevation height.

Although the models all show similar wind speed patterns there is a difference in the amount of wind speed streaks present and in the strength of the streaks. All the models show more intense streaks at the higher height. The LES models show more tendency for streaks than the RANS models. EllipSys3D shows almost no streaks whereas Alaya and OpenFoam CFDWind have similar streak patterns as the LES OpenFoam UUCG. The streaks correlate with topographical features, but there are also clear streaks in the PALM LES which ran without topography.

6   Discussion and Conclusions

All models except Meteodyn and PALM use ALS input for topography and forest data. Since a variety of different models, both LES and RANS, was able to use the ALS input this can be considered a success. The use of PAD data from ALS removes

the uncertainty of having to guess the PAD or the roughness length and displacement height, which in practice can be a larger source of uncertainty when estimating the wind resource at a potential site. The only model not to use the ALS derived PAD in some form was Meteodyn and that model also clearly stands out in the validation. Some of the difference may however also also be attributed to the use of different turbulence closure.

5   The majority of models consistently overpredict the shear and one may be led to believe that the forest representation, ALS conversion to PAD, is causing this discrepancy, but OpenFoam LES does in fact match the shear very well using the same forest data and the same C_d value. Especially interesting is the difference between OpenFoam LES and RANS, which is based on the same code and the same grid generator.

    The LES version of OpenFoam furthermore showed a much more pronounced difference between the inflow angles, both in 10 terms of shear and TKE, a possible explanation may be that the RANS models are overdiffusive, something also indicated by the fact that RANS models show less streaks in the horizontal planes.

    One of the most striking outcomes of the study is that the $k - \epsilon$ closure with standard constants produces far to little TKE. Also worth mentioning is the point that all of the RANS models (apart from Meteodyn) show a too high shear, in fact almost by a factor two in the upper layers, and therefore they would be expected to generate higher levels of TKE than found in the 15 measurements. This is also the case in 290° (Figure 6 (c)), but not in 100° where the shear also is too high in the upper parts.

    Two LES models took part in the study, and based on the validation, domain size seems more important than resolution. Since the low resolution OpenFoam LES captured the wind profile well for all heights and all directions it seems to be important to accurately model the PAD and topography in the footprint. That in turn means that domain size needs to be in the order of at least 20 km longitudinally.

20   When considering the accuracy of the modelling results one should also keep in mind the orders of magnitude different numerical challenge, both in the set up and the used computational time, using the different numerical approaches.

    A final note on the set-up of the benchmark. Many modellers expressed the difficulties involved in trying to determine the correct value of the U_g or pressure gradient in order to match the target 100 m wind speed. While it would be a possibility to instead normalise the results with, lets say, u_* or some other appropriate quantity, the fact that the upwind topography and PAD 25 seem crucial for good results point to the fact that normalisation may not be such a good idea since different wind speeds and turbulence levels would imply differences in the fetch.

Data availability. The data used to validate the models (selected as described in section 3) is available upon request. The PAD data is also available upon request

Author contributions. Stefan Ivanell coordinated the project. Johan Arnqvist selected the data, was responsible for the ALS to PAD conver-
30 sion, gathered the results and made the plots. Matias Avila ran Alaya, Dalibor Cavar ran EllipSys3D, Roberto Chavez ran CFDWind, Hugo

Olivares ran UUCGWind, Carlos Peralta and Jamal Adib ran Meteodyn and Björn Witha ran PALM. All authors contributed to writing the text

Acknowledgements. The work is mainly performed within the ERANET+ project NEWA. This work was partly conducted within StandUp for Wind, a part of the StandUp for Energy strategic research framework in Sweden. The simulations were partly performed on resources
5   provided by the Swedish National Infrastructure for Computing (SNIC) within the project SNIC 2017/11-10. Ebba Dellwik is greatly acknowledged for contributions regarding benchmark design, converting the ALS to PAD and measurement data selection.

References

PALM - A parallelized large-eddy simulation model for atmospheric and oceanic flows, http://palm.muk.uni-hannover.de.

WAsP digital maps formats, http://www.wasp.dk/Support-and-services/MapTypesList.

WindPro documentation, http://www.emd.dk/files/windpro/WindPRO_OnlineData.pdf.

5 OpenFOAM User Guide, https://cfd.direct/openfoam/user-guide/, 2015.

Apsley, D. D. and Castro, I. P.: A limited-length-scale k-ϵ model for the neutral and stably-stratified atmospheric boundary layer, Boundary-Layer Meteorology, 83, 75–98, doi:10.1023/A:1000252210512, https://doi.org/10.1023/A:1000252210512, 1997.

Arnqvist, J., Segalini, A., and Dellwik, E.: Wind Statistics from a Forested Landscape, Boundary-Layer Meteorology, pp. 53–71, doi:10.1007/s10546-015-0016-x, http://dx.doi.org/10.1007/s10546-015-0016-x, 2015.

10 Avila, M., Codina, R., and Principe, J.: Finite element dynamical subgrid-scale model for low Mach number flows with radiative heat transfer, International Journal of Numerical Methods for Heat & Fluid Flow, 25, 1361–1384, 2015.

Ayotte, K. W.: Computational modelling for wind energy assessment, Journal of Wind Engineering and Industrial Aerodynamics, 96, 1571–1590, doi:10.1016/j.jweia.2008.02.002, http://linkinghub.elsevier.com/retrieve/pii/S0167610508000317, 2008.

Bechmann, A.: Large-Eddy Simulation of Atmospheric Flow over Complex, Ph.D. thesis, Risø Technical University of Denmark, Roskilde, 15 Denmark, 2006.

Blackadar, A. K.: The vertical distribution of wind and turbulent exchange in a neutral atmosphere, Journal of Geophysical Research, 67, 3095–3102, doi:10.1029/JZ067i008p03095, http://dx.doi.org/10.1029/JZ067i008p03095, 1962.

Boudreault, L.-É.: Reynolds-averaged Navier-Stokes and Large-Eddy Simulation Over and Inside Inhomogeneous Forests, Ph.D. thesis, Technical University of Denmark, Department of Mechanical Engineering, 2015.

20 Boudreault, L. É., Bechmann, A., Tarvainen, L., Klemedtsson, L., Shendryk, I., and Dellwik, E.: A LiDAR method of canopy structure retrieval for wind modeling of heterogeneous forests, Agricultural and Forest Meteorology, 201, 86–97, doi:10.1016/j.agrformet.2014.10.014, 2015.

Cavar, D., Rthor, P.-E., Bechmann, A., Srensen, N., Martinez, B., Zahle, F., Berg, J., and Kelly, M.: Comparison of OpenFOAM and Ellip-Sys3D for neutral atmospheric flow over complex terrain, 1, 55–70, 2016.

25 Chávez-Arroyo, R., Sanz-Rodrigo, J., and Gancarski, P.: Modelling of atmospheric boundary-layer flow in complex terrain with different forest parameterizations, Journal of Physics: Conference Series, 524, doi:10.1088/1742-6596/524/1/012119, 2014.

Churchfield, M. J., Lee, S., and Moriarty, P. J.: Adding complex terrain and stable atmospheric condition capability to the OpenFOAM-based flow solver of the simulator for on/offshore wind farm applications (SOWFA), in: ITM Web of Conferences, vol. 2, EDP Sciences, 2014.

Codina, R.: Comparison of some finite element methods for solving the diffusion-convection-reaction equation, Computer Methods in Ap-30 plied Mechanics and Engineering, 156, 185 – 210, 1998.

Codina, R. and Soto, O.: Finite element implementation of two-equation and algebraic stress turbulence models for steady incompressible flows, Int. J. Num. Meth. Fluids, 30, 309–334, 1999.

Costa., J. C. P. L. D.: Atmospheric Flow over Forested and Non-Forested Complex Terrain., Ph.D. thesis, University of Porto, Porto, Portugal, 2007.

35 Crasto, G.: Forest Modeling. A canopy model for WindSim 4.5, University Lecture, 2006.

Deardorff, J.: Stratocumulus-capped mixed layers derived from a three-dimensional model, Boundary-Layer Meteorol., 18, 495–527, 1980.

Delaunay, D.: Meteodyn, http://www.meteodyn.com, 2007.

Delaunay, D.: Modelling the stable boundary layer for wind resource assessment, http://meteodyn.com/en/area/renewable-energies/wind-power-modelling-forecast-papers/#.WQwr62nyhaR, 2013.

Detering, H. W. and Etling, D.: Application of the E-ε turbulence model to the atmospheric boundary layer, Boundary-Layer Meteorology., 33, 113–133, 1985.

5 Enevoldsen, P.: Onshore wind energy in Northern European forests: Reviewing the risks, Renewable Sustainable Energy Reviews, 60, 1251–1262, doi:10.1016/j.rser.2016.02.027, 2016.

et al, M. V.: Alya: Multiphysics engineering simulation toward exascale, Journal of Computational Science, 14, 15 – 27, the Route to Exascale: Novel Mathematical Methods, Scalable Algorithms and Computational Science Skills, 2016.

Gargallo-Peiró, A., Avila, M., Owen, H., Prieto, L., and Folch, A.: Mesh generation for Atmospheric Boundary Layer simulation in wind
10 farm design and management, 124, 239–251, doi:https://doi.org/10.1016/j.proeng.2015.10.136, 2015.

Högström, U.: Review of some basic characteristics of the atmospheric surface layer, Boundary-Layer Meteorology, 78, 215–246, 1996.

Houzeaux, G., Aubry, R., and Vazquez, M.: Extension of fractional step techniques for incompressible flows: The preconditioned Orthomin(1) for the pressure Schur complement, Computers & Fluids, 44, 297 – 313, 2011.

Hurley, P.: An evaluation of several turbulence schemes for the prediction of mean and turbulent fields in complex terrain, Boundary Layer
15 Meteorology, 83, 43–73, 1997.

Jackson, S.: On the displacement height in the logarithmic velocity profile, Journal of Fluid Mechanics, 111, 15–25, 1981.

Kanani, F., Träumner, K., Ruck, B., and Raasch, S.: What determines the differences found in forest edge flow between physical models and atmospheric measurements? – An LES study, Meteorologische Zeitschrift, 23(1), 33–49, 2014.

Lantmäteriet: Tech. rep., Lantmäteriet, Sweden, https://www.lantmateriet.se/globalassets/kartor-och-geografisk-information/hojddata/
20 produktbeskrivningar/eng/lidar_data.pdf, 2016.

Launder, B. and Spalding, D.: The Numerical Computation of Turbulent Flow Computer Methods, 3, 269–289, 1974.

Lohner, R., Mut, F., Cebral, J. R., Aubry, R., and Houzeaux, G.: Deflated preconditioned conjugate gradient solvers for the pressure-Poisson equation: Extensions and improvements, International Journal for Numerical Methods in Engineering, 87, 2–14, 2011.

Mann, J., Angelou, N., Arnqvist, J., Callies, D., Cantero, E., Arroyo, R. C., Courtney, M., Cuxart, J., Dellwik, E., Gottschall, J., Ivanell, S.,
25 Kühn, P., Lea, G., Matos, J. C., Palma, J. M. L. M., Pauscher, L., Peña, A., Rodrigo, J. S., Söderberg, S., Vasiljevic, N., and Rodrigues, C. V.: Complex terrain experiments in the New European Wind Atlas, Philosophical Transactions of the Royal Society of London A: Mathematical, Physical and Engineering Sciences, 375, doi:10.1098/rsta.2016.0101, http://rsta.royalsocietypublishing.org/content/375/2091/20160101, 2017.

Maronga, B., Gryschka, M., Heinze, R., Hoffmann, F., Kanani-Sühring, F., Keck, M., Ketelsen, K., Letzel, M. O., Sühring, M., and Raasch,
30 S.: The Parallelized Large-Eddy Simulation Model (PALM) version 4.0 for atmospheric and oceanic flows: model formulation, recent developments, and future perspectives, Geosci. Model Dev., 8, 2515–2551, doi:10.5194/gmd-8-2515-2015, 2015.

Nebenführ, B.: Turbulence-resolving simulations for engineering applications, Ph.D. thesis, Chalmers University of Technology, Gothenburg, Sweden, 2015.

Panofsky, H. A., Tennekes, H., Lenschow, D. H., and Wyngaard, J. C.: The characteristics of turbulent velocity components in the surface
35 layer under convective conditions, Boundary-Layer Meteorology, 11, 355–361, doi:10.1007/BF02186086, 1977.

Paweł, G. and Roberto, C.-A.: Meshing procedure for the atmospheric wind flow modelling, doi:10.5281/zenodo.1000490, https://doi.org/10.5281/zenodo.1000490, 2017.

Richards, P. J. and Hoxey., R. P.: Appropriate boundary conditions for computational wind engineering models using the k-ϵ turbulence model, J. Wind Eng. Ind. Aerod., 46, 145–153, 1993.

Schumann, U.: Subgrid scale model for finite difference simulations of turbulent flows in plane channels and annuli, Journal of computational physics, 18, 376–404, 1975.

5   Shaw, R. H. and Schumann, U.: Large-eddy simulation of turbulent flow above and within a forest, Boundary-Layer Meteorol., 61, 47–64, 1992.

Sogachev, A. and Panferov, O.: Modification of Two-Equation Models to Account for Plant Drag, Boundary-Layer Meteorology, 121, 229–266, doi:10.1007/s10546-006-9073-5, https://doi.org/10.1007/s10546-006-9073-5, 2006.

Soto, O., Lohner, R., and Camelli, F.: A linelet preconditioner for incompressible flow solvers, International Journal of Numerical Methods

10   for Heat & Fluid Flow, 13, 133–147, 2003.

Watanabe, T.: Large-Eddy Simulation of Coherent Turbulence Structures Associated With Scalar Ramps Over Plant Canopies, Boundary-Layer Meteorology, 112, 307–341, 2004.

Weller, H. G., Tabor, G., Jasak, H., and Fureby, C.: A tensorial approach to computational continuum mechanics using object-oriented techniques, Computers in Physics, 12, 620–631, doi:10.1063/1.168744, 1998.

15   Yoshizawa, A.: Statistical theory for compressible turbulent shear flows, with the application to subgrid modelling, The Physics of Fluids, 29, 1986.

Yoshizawa, A. and Horiuti, K.: A statistically-derived subgrid-scale kinetic energy model for the large-eddy simulation of turbulent flows, Journal of the Physical Society of Japan, 54, 2834–2839, 1985.